Proceedings of the 20th International Conference on Soil Mechanics and Geotechnical Engineering– Rahman and Jaksa (Eds)

Numerical investigation of the long-term settlement behaviour of piled rafts in over-consolidated clay

Etude numérique du comportement de tassement à long terme de fondations en tables à piles dans de l'argile surconsolidée

Aljoscha Franzen & Oliver Reul
Department of Geotechnical Engineering, University of Kassel, Germany, A.Franzen@uni-kassel.de

ABSTRACT: In the scope of this paper the measured long term settlement behaviour of the Messeturm founded on a piled raft in overconsolidated Frankfurt Clay has been back-analyzed by means of three dimensional coupled pore pressure-displacement finite element analyses. Applying Mašín's hypoplastic material law which allows to consider creep effects for the Frankfurt Clay yielded reasonable agreement between measurements and analysis.

RÉSUMÉ : Dans le cadre de cet article, le comportement de tassement à long terme mesuré de la Messeturm fondée sur un radier de pieux dans l'argile surconsolidée de Francfort a été rétro-analysé au moyen d'analyses tridimensionnelles couplées par éléments finis de la pression et du déplacement des pores. L'application de la loi des matériaux hypoplastiques de Mašín, qui permet de prendre en compte les effets de fluage pour l'argile de Frankfurt, a permis d'obtenir un accord raisonnable entre les mesures et l'analyse.

KEYWORDS: numerical modelling, in-situ measurements, consolidation, visco-hypoplasticity, piled raft

1 INTRODUCTION

In recent decades an increasing number of structures have been founded on piled rafts allowing for an efficient reduction of settlements and differential settlements. Some of the earliest documented case histories of piled rafts, the Hyde Park Cavalry Barracks (Hooper 1973) and the Torhaus in Frankfurt, Germany (Sommer et al. 1985) have been carried out in overconsolidated clay. In overconsolidated Frankfurt Clay piled rafts have become the standard foundation solution, especially for high-rise buildings (e.g. Katzenbach et al. 2017).

The prediction of the time-dependent load-settlement behaviour of foundations in clayey soils is particularly important when existing and new foundation elements are to be integrated, which is becoming increasingly important, especially in inner-city areas (Butcher et al. 2006). Reul & Remmel (2009) report on the Parktower in Frankfurt where an existing high-rise building founded on a raft with an already significant deflection ratio of $\Delta/L = 1/340$ is heightened and the footprint extended by means of a piled raft. In order to be able to exploit further optimization potential by coupling existing foundations with new buildings, the time-dependent deformation behaviour of foundations must therefore also be taken into account to a greater extent. Thus, high requirements have to be applied to the modeling of the subsoil, since in cohesive soils both consolidation processes and the time-dependent material behavior (creep) have to be captured realistically.

In addition to the time-dependent deformation behaviour of the soil and variable building loads resulting from demolition and reconstruction phases, construction activities in the surrounding area also influence the long-term deformation behavior of foundations. In particular, the influence of neighbouring groundwater drawdowns has to be considered in this context. Owing to the frequently recurring changes in the groundwater table required for the construction of deep excavations or in connection with infrastructure construction measures, foundations in inner-city areas are subject to alternating stresses resulting from changes in the uplift and the effective stresses in the subsoil.

To investigate these topics this research work focuses on the well documented case history of the Messeturm in Frankfurt (e,g, Sommer & Hoffmann 1991a, Sommer et al. 1991). Reul & Randolph (2003) present the results of a detailed numerical back-analysis of the measurements on the Messeturm with a threedimensional finite element model where the nonlinear material behaviour of the soil was simulated with an elastoplastic cap-model, not considering time dependent effects such as consolidation and creep. Garcia et al. (2006) applied the viscohypoplastic material model by Niemunis (2003) in their back-analysis of the Messeturm without taking consolidation processes into account.

In the scope of this paper the available measurements on the Messeturm have been back-analyzed by means of three dimensional coupled pore pressure-displacement finite element analyses (FEA). Based on the results of oedometric and triaxial tests, the material behaviour of the Frankfurt Clay has been modelled with Mašín's hypoplastic material law (Mašín 2019a, 2019b) which allows to consider creep effects.

2 CASE HISTORY MESSETURM

The piled raft of the 256 m high Messeturm comprises 64 bored piles and a square raft with an edge length of 58.8 m. The length of the piles (diameter $d_p = 1.3$ m) varies from $L_p = 26.9$ m (outer ring), $L_p = 30.9$ m (middle ring) to $L_p = 34.9$ m (inner ring). The foundation level of the 3 m to 6 m thick raft lies 11 m to 14 m deep below ground level (Figure 1a). The construction of the building started in 1988 and was finished in 1991. Figure 2 shows the variation of the total settlement inducing building load with time which amounts to $P = G_{raft} + G + Q/3 = 1860$ MN.

The behaviour of the foundation was monitored from the construction period until more than seven years after the building was finished by means of geodetic and geotechnical measurements with 12 instrumented piles, 13 contact pressure cells, 1 pore pressure cell and 3 multi-point borehole extensometers. The positions of the measurement devices are plotted in the ground plan of the raft (Figure 1b).

For all 12 instrumented piles, the axial pile strains are measured in up to 11 planes by means of strain gauges. The pile head loads are measured on three of these piles with load cells at

the pile head. For the other 9 piles the pile loads have been derived from the strain measurements at the strain gauges placed immediately below the pile head and the pile axial stiffness. The mean Young's modulus of the piles of E_{pile} = 25000 MPa has been derived from the in-situ measurements (Reul 2000). Since the pile loads are calculated from strain measurements, the pile loads presented in this paper as well as by Reul & Randolph (2003) are smaller than the values previously published (Sommer et al. 1990 & 1991, Sommer & Hoffmann 1991a & b, Sommer 1993) where a Young's modulus of the pile concrete alone of $E_{concrete}$ = 30000 MPa is assumed (Sommer & Hoffmann 1991a).

For the construction of a subway tunnel with a station 47 m east of the Messeturm, groundwater had to be drawn down more than 12 m at the tunnel (Sommer et al. 1991). As a result, the groundwater level in the vicinity of the Messeturm decreased about 10 m, which led to changes of the uplift on the raft of 287 MN. During the construction process of the subway tunnel and the station the groundwater lowering was suspended for 2 years and continued in 1994 until the end of 1996. Figure 9e & b shows the variation of the groundwater level and the average measured pile resistances for the inner, middle and outer pile ring with time. A groundwater drawdown is accompanied by an increase of the pile resistances and a groundwater rise by a decrease of the pile resistances, respectively, as will be discussed in section 5.

If not indicated otherwise, all measurements presented in the scope of this paper have been adapted from Reul (2000) who re-evaluated the data published by Sommer et al. (1990 & 1991), Sommer & Hoffmann (1991a & b) and Sommer (1993) for the construction process and carried out long-term measurements.

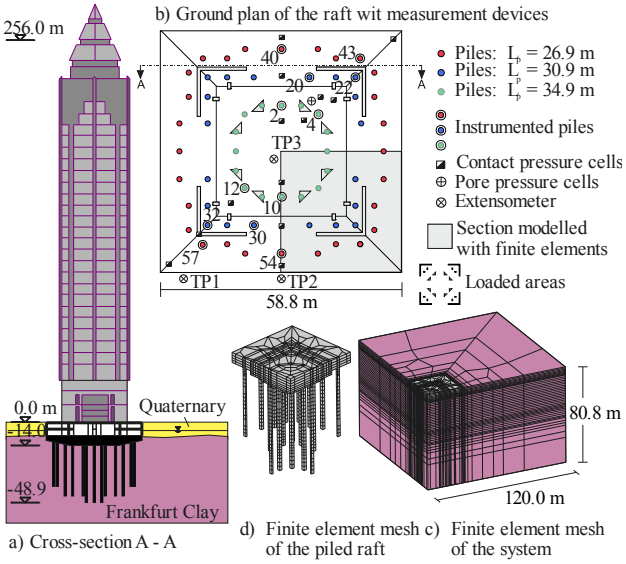

Figure 1. Messeturm, Frankfurt.

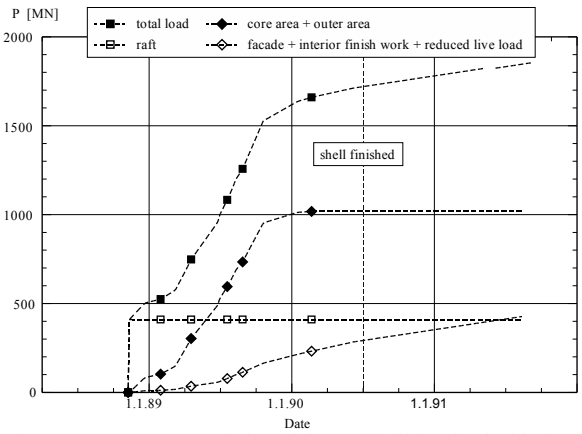

Figure 2. Messeturm: Variation of the total building load with time.

3 SUBSOIL CONDITIONS

The subsoil condition in Frankfurt am Main, Germany, is characterised mainly by tertiary soils and rock. They consist of Frankfurt Clay at the top underlain by the rocky Frankfurt Limestone. The Frankfurt Clay is a stiff, overconsolidated clay with its characteristics liquid limit, plastic index and natural moisture content very similar to the London Clay (Butler 1975). Sand and limestone bands of varying thickness are embedded in the Frankfurt Clay, which results in a nonhomogenous appearance of the layer as a whole. The compressibility of the Frankfurt Limestone, which is composed of massive limestone and dolomite layers, algal reefs, marly calcareous sands and silts and marly clay, is small compared to the Frankfurt Clay.

The groundwater circulates in the quaternary sand and gravel as well as in the tertiary sand and limestone bands while the tertiary clay is practically impermeable. Because the quaternary and tertiary aquifers are connected, a groundwater drawdown in the tertiary layers may result in a reduction of the hydraulic head within an area with a radius of several hundred meters.

Taking into account correlations documented in the literature (e.g. Dolinar 2009, Kozlowski & Ludynia 2019) the permeability of the clay can be estimated to range between $k = 10^{-14}$ m/s to $k = 10^{-9}$ m/s. Preliminary laboratory tests conducted in the scope of this research work resulted in a permeability of $k = 1.4 \cdot 10^{-11}$ m/s for the clay. However, for the estimation of the consolidation behaviour of the Frankfurt Clay, the system permeability of the entire stratum is of great importance. Due to the heterogeneous stratification of the Frankfurt Clay and the strongly varying proportion of sand and limestone bands, which are decisive for drainage, large site-specific deviations are possible.

In the vicinity of the Messeturm the subsoil consists of fill and quaternary sand and gravel up to a depth of 10 m below ground level, which is followed by the Frankfurt Clay up to a depth of at least 70 m below ground level. The groundwater level is situated 4.5 m to 5.0 m below ground level. The evaluation of two 71.3 m and 50.0 m deep borehole logs available for the Messeturm site showed shares of sand and limestone bands in the overall profile in a range of 4.4 % to 12.2 % (sand) and 8.8 % to 9.5 % (limestone), respectively.

4 NUMERICAL MODEL

4.1 *Finite element model*

The numerical study was carried out by means of three dimensional finite element analyses (FEA) with the code Tochnog (Tochnog Professional Company 2020). With the coupled pore pressure-displacement analyses the time dependent displacement caused by consolidation processes as well as by the material behaviour of the soil is modelled. The finite element mesh comprises 13650 hexahedral elements with both displacements and pore pressures varying linearly across the elements.

Figure 1c shows the finite element mesh of the system where 1/4 of the complete 3D problem has been modelled considering the two symmetry planes of the structure. The boundary between the Frankfurt Clay and the Frankfurt Limestone which represents the bottom of the finite element mesh has been assumed to be 74.8 m below the bottom of the raft. Only the soil below the top surface of the raft is modelled with finite elements. The soil above this level is considered through its weight.

Figure 1d shows the detail of the piled raft. The thickness of the raft decreases in three steps from the core area (t_r = 6 m) to the edge of the raft (t_r = 3.0 m). The circular piles have been replaced by square piles with the same shaft circumference. For the modelling of the contact zone between soil and the large diameter bored piles, thin solid continuum elements have been applied instead of special interface elements. The contact between structure and soil was described as perfectly rough. This means that no

relative motion between the nodes of the finite elements that represent the structure and those of the finite elements that represent the soil takes place. The material behaviour in the contact area was simulated by the material behaviour of the soil. A discussion of the influence of the mesh refinement on the results of the FEA of piled rafts can be found in Reul & Randolph (2002).

The material behaviour of the Frankfurt Clay has been modelled with Mašín's hypoplastic model (Mašín 2019a, 2019b). The determination of the relevant material parameters for the Frankfurt Clay are discussed in section 4.2. The piles and the raft are considered to behave linear-elastically with the material parameters summarized in Table 1.

Table 1. Material parameters for piles and raft used in the FEA

	Unit weigth		Young's modulus	Poisson's ratio
	γ [kN/m³]	γ' [kN/m³]	E [MN/m²]	ν [-]
Piles	25	15	25000	0.20
Raft	25	15	34000	0.20

For the coupled displacement-pore pressure FEA carried out, it is assumed that the pore fluid flow is governed by Darcy's law, that the soil pores are fully saturated ($S_r = 1$) and that the pore fluid (water) is incompressible. Drainage of the soil takes place beneath the raft as well as at every model surface except for the symmetry axes. The piles are assumed to be impermeable.

Table 2 summarizes the step-by-step analysis of the construction process. The piles have been modelled "wished-in-place", i.e. changes in the soil surrounding the pile caused by the installation process have not been modelled. The total dead weight of the raft of G_{raft} = 410 MN has been modelled as a gravity load. The total settlement inducing load of the superstructure of P = G+Q/3 = 1445 MN has been applied on top of the raft in the areas of walls and columns (Figure 1b). The groundwater level is controlled by a defined hydraulic pressure head at the drainage surfaces mentioned above. Groundwater level changes are then performed by changing the hydraulic pressure head.

Table 2. Step-by-step analysis of the construction process in the FEA

Step		P [MN]	GW [masl]	Δt [d]	Date
1	In situ stress state	-	92.5	-	´-
2	Start GW drawdown	-	92.5/90.9	17	26.06.88
3	Excavation to 7.5 m below ground level	-	90.9/89.0	22	13.07.88
4	Pile installation	-	89.9/86.1	32	04.08.88
5	Excavation to 14.0 m below ground level	-	86.1/83.4	52	05.09.88
6	Application of weight of raft	410	83.4/83.0	12	29.10.88
7	Application of raft stiffness	410	83.0	1	10.11.88
8	Loading + GW management	1860	83.0/92.4/ 83.0	998	11.11.88
9	GW management	1860	83.0/93.2/ 83.5/92.5	2681	06.08.91
10	Consolidation + creep	1860	92.5	14433	08.12.98

P total settlement inducing load (G_{raft}+G+Q/3)
GW ground water level in m above sea level
Δt duration of process
Date starting date

4.2 Material parameters for the Frankfurt Clay

In order to model time-dependent material behavior, the material model according to Mašín (2019a, 2019b) is used in this work. In its basic version the constitutive law is a hypoplastic model defined by the following equation:

$$\dot{\sigma} = \underbrace{\boldsymbol{L}:\dot{\boldsymbol{\varepsilon}}}_{\text{Linear}} + \underbrace{\boldsymbol{N}\|\dot{\boldsymbol{\varepsilon}}\|}_{\text{Nonlinear}} \qquad (1)$$

where $\dot{\boldsymbol{\sigma}}$ = stress rate; $\dot{\boldsymbol{\varepsilon}}$ = strain rate; $\boldsymbol{L}$ = linear stiffness tensor of fourth order and $\boldsymbol{N}$ = non-linear stiffness tensor of second order.

In its basic form Mašín's law is a rate-independent material model based on an explicit asymptotic state boundary surface approach. It requires the specification of the five soil parameters (e.g. φ_c, N, λ^*, κ^*, ν) similar to the Cam-Clay model. To implement rate dependency the nonlinear part of the basic equation is replaced by the approach of Niemunis (2003):

$$\dot{\sigma} = f_s \boldsymbol{L}:\dot{\boldsymbol{\varepsilon}} - D_r\left(\frac{1}{OCR}\right)^{\frac{1}{I_v}} A:\boldsymbol{d} \qquad (2)$$

where A = asymptotic state boundary surface, **d** = asymptotic direction of strain rate, f_s = Scalar factor to account for stress dependency, I_v = viscosity index; D_r = reference creep rate.

Mašín's hypoplastic material law (Mašín 2019a, 2019b) allows to model viscous soil behaviour. However, it has to be noted that capturing cyclic loading with this approach poses some difficulties since all nonlinear deformations are defined rate-dependent in the model. Moreover, the formulation becomes almost elastic for high OCR values. This issue was addressed by Niemunis et al (2009), who modified the viscous term to include irreversible behavior inside the state boundary surface.

To investigate the material behaviour of the clay fraction of the Frankfurt Clay, so far 18 oedometer tests, 10 consolidated undrained (CU) and 2 consolidated drained (CD) triaxial tests on clay samples obtained from various project sites in Frankfurt have been carried out at the University of Kassel. Additionally, 4 oedometer tests and 19 CD triaxial tests carried out during the site investigation for the Messeturm have been re-evaluated in the scope of this research work. As an example Figure 3 shows the numerical simulation of an oedometer test indicating that Mašín's hypoplastic model is suited to capture the deformation behaviour of the clay samples.

From the oedometers tests a slope of $\lambda^* = 0.0670$ for the isotropic compression line and a slope of $\kappa^* = 0.0140$ for the isotropic unloading line have been determined with $\lambda^*/\kappa^* \approx 5$. In order to capture the effect of the increased stiffness of limestone and sand bands in the FEA the two parameters have been modified to $\lambda^* = 0.0160$ and $\kappa^* = 0.0032$ for the Frankfurt Clay keeping the ratio λ^*/κ^* as evaluated in the oedometer tests. Additionally, from the oedometer tests on the clay samples the viscosity index has been determined to $I_v = 0.03$. Figure 4 shows the development of the viscosity depending on the load level for the example of one test. For each test the viscosity index has been evaluated as the mean value of all load stages with OCR = 1.

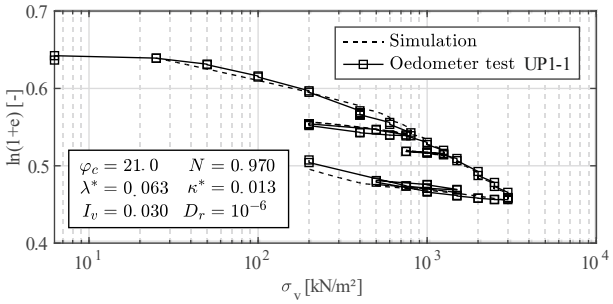

Figure 3. Numerical simulation of an oedometer test on a clay sample using Mašín's hypoplastic model.

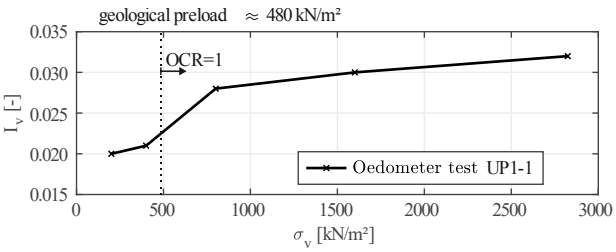

Figure 4. Evaluation of the viscosity index from oedometer tests.

Figure 5a compares the depth profiles of the earth pressure at rest established by Franke et al. (1985) and Mader (1989) with the approach applied in the FEA. According to Mader (1989), the coefficient of earth pressure at rest ranges from $K_0 = 0.72$ at z = 10 m below ground surface to $K_0 = 0.57$ at a depth of

z = 35 m. In the FEA the earth pressure at rest is assumed to decrease linearly from $K_0 = 0.72$ at a depth of z = 10 m below ground surface to $K_0 = 0.64$ at a depth of z = 37 m and remaining constant from there on.

Data on the overconsolidation ratio provided by Mader (1989) and Franke et al. (1985) is plotted in Figure 5b together with results from oedometer test from the site investigation for the Messeturm. In the FEA the approach by Franke et al. (1985) was used because of its reasonable agreement with the tests results.

Based on the results of the triaxial tests, the critical angle of friction is assumed to vary linearly with depth (Figure 5c). Further tests with samples obtained from larger depth will be carried out in the future to verify this hypothesis.

The Poisson's ratio which regulates the shear stiffness (Mašín 2019a) has been derived from the back-analyses of triaxial tests to $\nu = 0.25$. For the reference creep rate a typical value of $D_r = 10^{-6}$ s^{-1} has been selected.

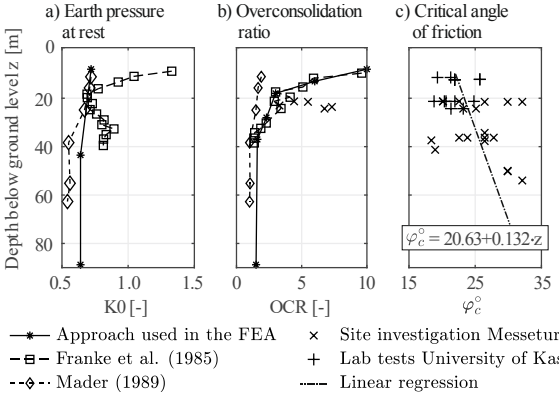

Figure 5. Depth profiles of earth pressure at rest, overconsolidation ratio and critical angle of friction.

The material parameters for Mašín's hypoplastic model used in the FEA for the Frankfurt Clay, approximating the influence of the sand and limestone bands on the overall stiffness of the layer, are summarized in Table 3.

Table 3. Material parameters for Mašín's hypoplastic model used for the Frankfurt Clay in the FEA

Parameter			
Total unit weight	γ	[kN/m³]	18.5
Buoyant unit weight	γ'	[kN/m³]	8.5
Critical angle of friction	φ_c	[°]	20.63+0.132·z
Position of the isotropic compression line	N	[-]	0.970
Slope of the isotropic compression line	λ^*	[-]	0.0160
Slope of the isotropic unloading line	κ^*	[-]	0.0032
Poissons's ratio	ν	[-]	0.25
Reference creep rate	D_r	[s^{-1}]	10^{-6}
Viskosity index	Iv	[-]	0.03
Overconsolidation ratio	OCR	[-]	1.4-6.0
Coefficient of earth pressure at rest	K_0	[-]	0.64-0.72

z Depth below ground surface [m]

4.3 *System permeability for the Frankfurt Clay*

For the numerical simulations it is convenient to replace the heterogenous Frankfurt Clay (Figure 6a) with its embedded limestone and sand bands of varying thickness with a homogenous soil mass and an appropriate equivalent system permeability (Figure 6b). Taking a permeability of $k_{clay} = 1.4 \cdot 10^{-11}$ m/s for the clay and a significantly higher permeability ($\geq 1 \cdot 10^{-4}$ m/s) for the limestone and sand bands into account, the system permeability k_{system} can be estimated applying the 1-dimensional consolidation theory (Terzaghi & Fröhlich 1936) as follows:

$$k_{system} = k_{clay} \left(\frac{h_{system}}{h_{clay}} \right)^2 \qquad (3)$$

where k_{clay} = permeability of clay; h_{clay} = characteristic length of dewatering in the Frankfurt Clay (Figure 6c; half distance between neighbouring permeable layers, i.e. limestone and sand bands); h_{system} = characteristic length of dewatering in the finite element model.

The evaluation of the two available borehole logs from the Messeturm site yield an average distance between permeable layers (limestone and sand bands with a thickness d ≥ 0.5 m) of $h_{clay,ave} = 5.8$ m and maximum distance of $h_{clay,max} = 12.8$ m. With $h_{system} = 37.4$ m (half distance between the bottom of the raft and the bottom surface of the finite element mesh) the system permeability can be estimated to be in a range of $k_{system} = 5.8 \cdot 10^{-10}$ m/s to $k_{system} = 1.2 \cdot 10^{-10}$ m/s.

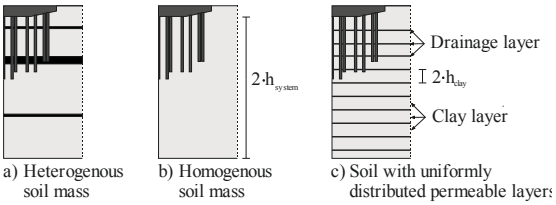

Figure 6. Determination of a system permeability for the Frankfurt Clay.

Figure 7 compares the measured variation of settlement with time with the FEA results for the three different models depicted in Figure 6. For the heterogenous soil mass the distribution of permeable layers has been approximated from the two available borehole logs from the Messeturm site. For relatively closely spaced permeable layers a significant increase of settlements during the construction phase can be observed (Figure 7: model according to Figure 6c, $h_{clay} = 3.5$ m). For the homogenous soil mass with a system permeability of $k_{system} = 1.5 \cdot 10^{-10}$ m/s a reasonable agreement with the measurements can be achieved.

Figure 8 shows the results of a sensitivity analysis of the system permeability for the FEA with a homogenous soil mass (Figure 6b). In a range of $k_{system} = 1.0 \cdot 10^{-10}$ m/s to $k_{system} = 2.0 \cdot 10^{-10}$ m/s the measured variation of settlements with time is captured reasonably well.

In the remainder of this paper a homogeneous soil mass as depicted in Figure 6b with a system permeability for the Frankfurt Clay of $k_{system} = 1.5 \cdot 10^{-10}$ m/s has been applied.

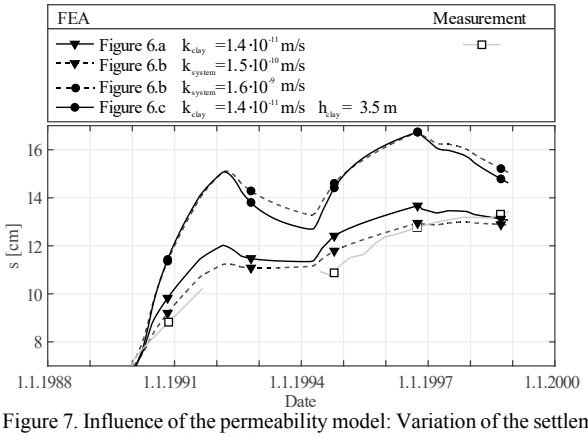

Figure 7. Influence of the permeability model: Variation of the settlement at the centre of the raft with time.

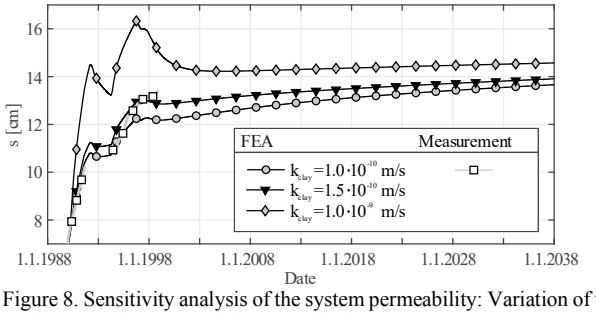

Figure 8. Sensitivity analysis of the system permeability: Variation of the settlement at the centre of the raft with time.

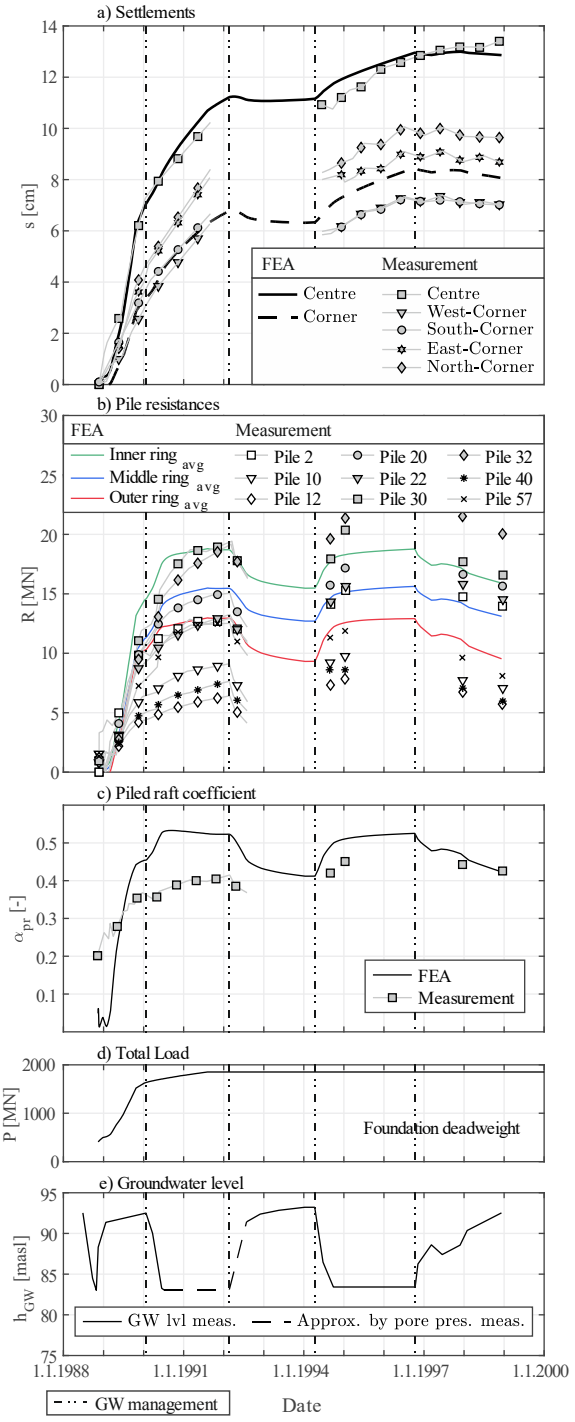

Figure 9. Variation of settlements, pile resistances, piled raft coefficient, load and groundwater level with time.

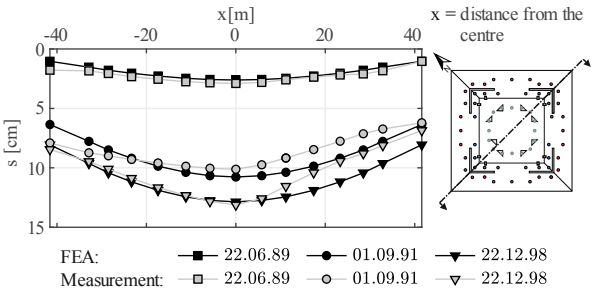

Figure 10. Distribution of settlements in the cross section of the raft.

5 COMPARISON OF IN-SITU MEASUREMENTS AND NUMERICAL ANALYSIS

Figure 9 compares the measured variation of settlements, pile resistances and piled raft coefficient with time with the results of the FEA. Additionally, the development of the total load of the building and the groundwater level with time are shown. Due to the location of the groundwater drawdown for the subway tunnel (see chapter 2) north-east of the Messeturm, the settlements at the northern and eastern corner are slightly higher than at the southern and western corner (Figure 9a). This influence is also visible in Figure 10 where the settlements in a cross section running in east-west-direction are plotted. However, since the finite element model is restricted to 1/4 of the foundation this effect is not captured in the FEA.

The changes of the groundwater level, and the resulting uplift on the raft, caused alterations of the pile resistances of up to 3 MN (Figure 9b). A groundwater drawdown is accompanied by an increase of the pile resistances and a groundwater rise by a decrease of the pile resistances, respectively.

The piled raft coefficient presented in Figure 9c describes the ratio of the sum of all pile resistances ΣR_{pile} to the total resistance of the foundation, R_{tot}:

$$\alpha_{pr} = \frac{\Sigma R_{pile}}{R_{tot}} \qquad (4)$$

For the piled raft coefficient the finite element analysis yields $\alpha_{pr} = 0.52$ (groundwater draw down) and $\alpha_{pr} = 0.43$ (natural groundwater level), respectively. Based on the assumption that the average pile resistance can be derived from the 12 instrumented piles, the piled raft coefficient at the time of the last documented measurement, where the ground water is situated almost at its natural level, is $\alpha_{pr} = 0.43$.

Figure 11 shows the average pile load distribution along the pile shaft for the outer pile ring ($L_p = 26.9$ m), the middle pile ring ($L_p = 30.9$ m) and the inner pile ring ($L_p = 34.9$ m) at three different dates. While measurements and FEA are in reasonable agreement for the outer and the middle pile ring, the FEA appears to overestimate the pile loads for the inner pile ring. However, the uncertainties concerning the estimation of the Young's modulus for the piles need to be kept in mind (see chapter 2).

A comparison of the measured and calculated settlement profiles at the extensometers TP1 and TP3 (Figure 1b) is plotted in Figure 12. For both extensometers reasonable agreement between measured and calculated settlement profiles is achieved.

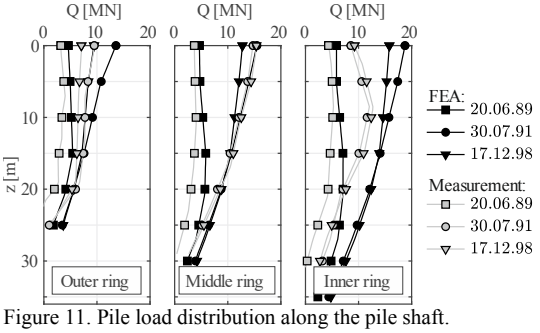

Figure 11. Pile load distribution along the pile shaft.

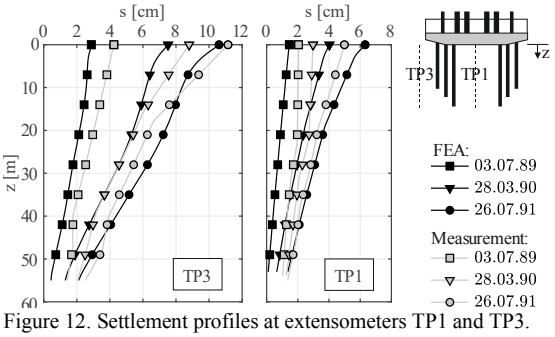

Figure 12. Settlement profiles at extensometers TP1 and TP3.

Figure 13 shows the results of a sensitivity analysis of the viscosity index which controls the creep deformations. While a viscosity index of $I_v = 0.025$ yields only creep settlements of $s \approx 0.2$ cm over a time period of 40 years, the creep settlements increase to $s \approx 2.7$ cm for $I_v = 0.035$.

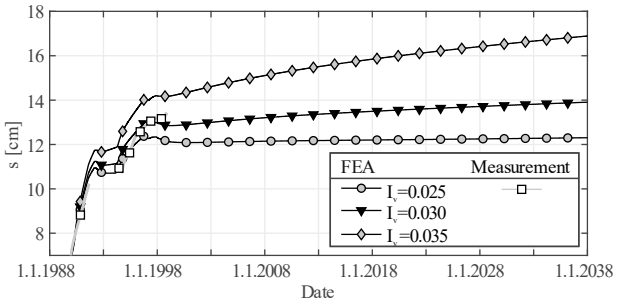

Figure 13. Sensitivity analysis of the viscosity index: Variation of the settlement at the centre of the raft with time.

6 CONCLUSIONS

The three dimensional coupled pore pressure-displacement FEA carried out for the back-analysis of the Messeturm applying Mašín's hypoplastic material for the Frankfurt Clay provided reasonable agreement with the measured long-term behaviour of the piled raft. Replacing the heterogeneous Frankfurt Clay with its embedded limestone and sand bands by a homogeneous soil mass with an equivalent system permeability proved to be an efficient strategy for modelling consolidation effects.

The next steps in the research project will focus on the application of the AVISA model (Tafili & Triantafyllidis 2020) for the back-analysis of further case histories in Frankfurt Clay. The AVISA model allows for a more realistic simulation of alternating stresses caused by complex loading histories. For this reason, additional triaxial and oedometer tests on samples from Frankfurt Clay will be carried out to establish the material parameters of the AVISA model.

ACKNOWLEDGEMENTS

The authors would like to thank CDM Smith Consult GmbH, Ingenieursozietät Professor Dr.-Ing. Katzenbach GmbH and Prof. Quick und Kollegen Ingenieure und Geologen GmbH for providing samples of Frankfurt Clay for the lab tests. The historical data of the Messeturm site investigation (results of lab tests and borehole logs) has been provided by CDM Smith Consult GmbH.

The overall project is funded by the Deutsche Forschungsgemeinschaft (DFG, German Research Foundation) - RE 3881/4-1.

6 REFERENCES

Butcher A.P., Powell J.J.M. and Skinner H.D. 2006. Reuse of foundations for urban sites - a best practice handbook. IHS BRE Press, Bracknell.

Butler F.G. 1975. Heavily over-consolidated clays - Review paper: Session III. Proc. Conf. Settlements of Structures, Cambridge, 531-578.

Dolinar B. 2009. Predicting the hydraulic conductivity of saturated clays using plasticity-value correlations. Applied Clay Science, 45, 90-94.

Franke E., Mader H., Schetelig K. and Schneewolf T. 1985. Anisotropie des Eigenspannungszustandes der wechsellagernden Locker- und festgesteinsschichten des Frankfurter Raumes. In: Ingenieurgeologische Probleme im Grenzbereich zwischen Locker- und Festgesteinen – Heitfeld (Hrsg.), 399-416, Berlin, New York Springer-Verlag, ISBN : 978-3-540-15366-5.

Garcia F., Lizcano A. and Reul O. 2006. Numerical modelling of the case history of a piled raft with a viscohypoplastic model. In: Numerical Modelling of Construction Processes in Geotechnical Engineering for Urban Enviroment – Triantafyllidis (ed), 265-271, Taylor & Francis Group, London, ISBN: 0415397480.

Hooper, J. A. 1973. Observations on the behaviour of a piled-raft foundation on London Clay. Proc. ICE, Part 2, Vol. 55, 855-877

Katzenbach R., Leppla S. and Choudhury D. 2017. Foundation Systems for High-Rise Structures. CRC Press.

Kozlowski T. and Ludynia A. 2019. Permeability coefficient of low permeable soils as a single-variable function of soil parameter. Water, 11, 2500, doi:10.3390/w11122500.

Mader H. 1989. Untersuchungen über den Primärspannungszustand in bindigen überkonsolidierten Böden am Beispiel des Frankfurter Untergrundes. Mitteilungen des Institutes für Grundbau, Boden- und Felsmechanik der TH Darmstadt, Heft 29.

Mašín D. 2019a. Hypoplastic Model for Clay. In: Modelling of Soil Behaviour with Hypoplasticity, 103-117, Springer Series in Geomechanics and Geoengineering. Springer, Cham. https://doi.org/10.1007/978-3-030-03976-9_6.

Mašín D. 2019b. Advanced Modelling Approaches. In: Modelling of Soil Behaviour with Hypoplasticity, 132-142 Springer Series in Geomechanics and Geoengineering. Springer-Verlag, Cham. https://doi.org/10.1007/978-3-030-03976-9_7.

Niemunis A. 2003. Extended hypoplastik models for soils. Schriftenreihe des Institutes für Grundbau und Bodenmechanik der Ruhr-Universität Bochum, Band 34.

Niemunis A., Grandas-Tavera C.E. and Prada-Sarmiento L.F. 2009. Anisotropic visco-hypoplasticity. Acta Geotechnica 4, 293-314. https://doi.org/10.1007/s11440-009-0106-3.

Reul O. 2000. In-situ-Messungen und numerische Studien zum Tragverhalten der Kombinierten Pfahl-Plattengründung. Mitteilungen des Institutes und der Versuchsanstalt für Geotechnik der technischen Universität Darmstadt, Heft 53.

Reul O. and Randolph M.F. 2002. Study of the influence of finite element mesh refinement on the calculated bearing behaviour of a piled raft. Proc. 8th International Symposium on Numerical Models in Geomechanics, 259-264.

Reul O. and Randolph M.F. 2003. Piled rafts in overconsolidated clay – Comparison of in-situ measurements and numerical analyses. Géotechnique, 53, No. 3, 301-315.

Reul O. and Remmel G. 2009. Foundation design for the extension of an existing high-rise building. Proc. 17th Int. Conference on Soil Mechanics and Geotechnical Engineering, Alexandria, Hrsg: Hamza, M., Shahien, M., El-Mossallamy, Y., Vol. 2, 2072-2075.

Sommer H. 1993. Development of locked stresses and negative shaft resistance at the piled raft foundation - Messeturm Frankfurt/Main. Proc. Deep Foundations on Bored and Auger Piles, 347-349, Rotterdam: Balkema.

Sommer H. and Hoffmann H. 1991a. Load-settlement behaviour of the fairtower (Messeturm) in Frankfurt/Main. Proc. 4th International Conference on Ground Movements and Structures, 612-627, London: Pentech Press.

Sommer H. and Hoffmann H. 1991b. Last-Verformungsverhalten der Gründung des Messeturmes Frankfurt/Main. Festkolloquium 20 Jahre Grundbauinstitut Prof. Dr.-Ing. H. Sommer und Partner, 63-71.

Sommer H., Wittmann P. and Ripper P. 1985. Piled raft foundation of a tall buiding in Frankfurt clay. Proc. 11th ICSMFE, San Francisco, Vol. 4, 2253-257, Rotterdam: Balkema.

Sommer H., Katzenbach R. and DeBenedittis C. 1990. Last-Verformungsverhalten des Messeturms Frankfurt/Main. 21.Baugrundtagung der Deutschen Gesellschaft für Geotechnik in Karlsruhe, 371-380.

Sommer H., Tamaro G. and DeBeneditis C. 1991. Messe Turm, foundations for the tallest building in Europe. Proc. 4th International Conference on Piling and Deep Foundations, 139-145, Rotterdam: Balkema.

Tafili M., and Triantafyllidis T. 2020. AVISA: anisotropic visco-ISA model and its performance at cyclic loading. Acta Geotech. 15, 2395–2413. https://doi.org/10.1007/s11440-020-00925-9.

Terzaghi K. and Fröhlich O.K. 1936. Theorie der Setzung von Tonschichten – Eine Einführung in die analytische Tonmechanik; Deuticke, Leipzig und Wien.

Tochnog Professional Company 2020. TOCHNOG PROFESSIONAL - User's manual. https://www.tochnogprofessional.nl, Last access on Dec. 7th 2020.